# MODELING THE INTERACTION OF MULTIBEAM/MULTIMODE ULTRASONIC TRANSDUCERS WITH FATIGUE CRACKS IN CLADDED REACTOR PRESSURE VESSELS

George Gruber and Ted Mueller

Southwest Research Institute
6220 Culebra Road
San Antonio, TX 78284

## INTRODUCTION AND PROBLEM STATEMENT

The integrity of reactor pressure vessels is primarily affected by the presence of fatigue cracks. The novel SLIC transducers which simultaneously use Shear and Longitudinal waves for material Inspection and flaw Characterization have recently been qualified in conjunction with satellite-pulse flight time measurement techniques on over fifty fatigue cracks in cladded test blocks [1]. However, a computer modeling capability to aid the ultrasonic examiner in the interpretation of the data was not available during the 1983-84 qualification trials of the multibeam inspection (SLIC) technology [1].

## OBJECTIVES AND APPROACH

In 1986 [2], full elastodynamic theory was applied to account for the echo structure and dynamics of the composite pulse patterns obtained for a fatigue crack with the SLIC-40 multibeam detection transducer and the SLIC-50 multimode sizing transducer. As a result, the arrival times of the satellite pulses relative to those of the main pulses were predicted for crack sizing with typical errors of less than 5 percent. The solution of the inverse problem was, however, hindered by the inclusion in the formulation of the direct problem, the effects of the probe directivity functions and crack diffraction coefficients on the pulse amplitudes and flight times. The objectives of this work were to derive and validate three sets of flight-time formulas for the SLIC-40/50/30 pulse patterns which can be readily inverted for the accurate estimation of crack depth and location. To accomplish these objectives, we set out to

(1) Neglect the effects of the crack diffraction coefficients on the pulse flight times,

(2) Remove the effects of the probe characteristics on the pulse flight times by calibrating the instrument screen's time base with a set of known omnidirectional reflectors, and

(3) Base the prediction of the variation of pulse flight times $T_i$ (i=1, 2, or 3) with transducer position X for a given crack

location $Z_1$ and crack depth d ($=Z_2-Z_1$) on the sound-path-tracing models postulated in [1] and [2].

## SOLUTION OF THE DIRECT PROBLEM

### The Multibeam SLIC-40 Transducer

As shown in Fig. 1(a), the cracks of interest are contained in planes that are nearly perpendicular to the cladded inspection surface (IS at Z=0). The SLIC-40 was especially designed to improve the detection reliability of near-surface cracks ($Z_1 < 50$ mm) by directing its converging L-beams ($L_a$ and $L_b$) toward the upper crack extremity located at $Z_1$ [see the left part of Fig. 1(b)]. All crack detection, identification (confirmation), and sizing measurements are made with the diffracted pulses from the upper and lower crack extremities [pulses 1 and 2 in Fig. 1(b)].

Crack sizing in the through-wall (Z) direction is a secondary function of the SLIC-40. Fig. 1(a) actually shows the SLIC-40 in its traditional crack-sizing position $X_2$ [see also the right part of Fig. 1(b)] where the amplitude $A_2$ of the crack-depth-information-carrying signal ("satellite" or pulse 2) is maximum. The unknown dependence of $\tau_2$ on $Z_1$, in addition to its dependence on d($=Z_2-Z_1$), has necessitated in the past the fabrication of expensive calibration blocks containing notches of varying depth at the potential $Z_1$ locations to aid in the crack-sizing process. The equations and theoretical TX or PX plots (pulse position P on the screen plotted against transducer position X on the surface irrespective of pulse amplitude) derived below not only result in significant block fabrication cost savings but also permit partial automation of the complex flaw characterization process.

Fig. 2 shows the three sound paths (rays bf, fa, and ba) postulated for the strongest (L-to-L wave) interaction of the SLIC-40 with a side-drilled hole. Only the direct sound path (ray R) is involved in the interaction of the SLIC-40 with a flaw located at Z=0 (e.g., a surface scratch). The surface-skimming (lateral) wave pulse corresponding to the direct sound path serves as a calibration signal marking the origin of the time base of the instrument screen (T=0, P=0, or Z=0). The arrival time of the reference pulse is given by

$$T_r = R/c \tag{1}$$

where c is the L-wave velocity. The variation of the flight time of the L-wave reflected by the hole (pulse 1) relative to the arrival time of the reference pulse with transducer position is calculated from

$$T_1\ (X;\ Z_o) = (U + V - R)/c \text{ in } \mu s \tag{2}$$

where

$$U\ (X;\ Z_o) = (Z_o^2 + X^2)^{1/2} \tag{2a}$$

and

$$V\ (X;\ Z_o) = \left[Z_o^2 + (X - R)^2\right]^{1/2}. \tag{2b}$$

For the SLIC-40 used in the model-development experiments, the variation of the position of pulse 1 against the 50-mm wide instrument screen with transducer position X for a given reflector location $Z_o$ is predicted by

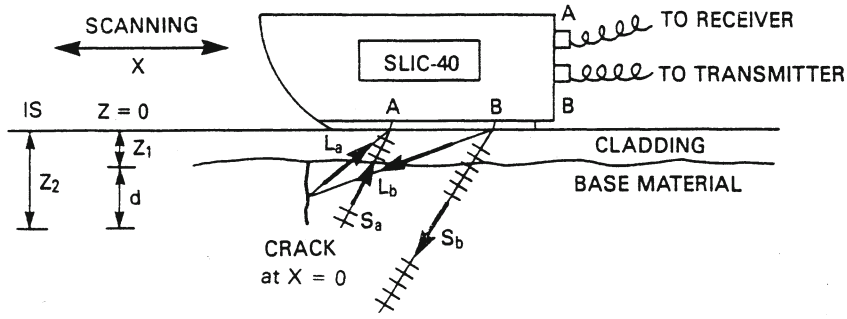


(a) Transmitted ($L_b$, $S_b$) and received ($L_a$, $S_a$) beams.

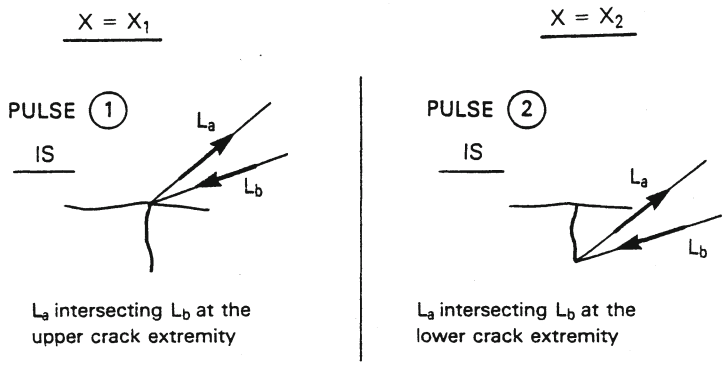


(b) Two pulses returned by an underclad crack.

Fig. 1. Interaction of the transmitted 70-degree longitudinal wave ($L_b$) of the SLIC-40 with an underclad crack resulting in four edge-diffracted pulses (one L-wave and one S-wave from each crack extremity). These pulses are labeled 1L or 1, 1S, 2L or 2, and 2S. The S-wave pulses are generally not observed.

$$P_1 (X; Z_o) = 0.308 (U + V - R) \quad \text{in mm} \tag{3}$$

where R is allowed to vary between 14.5 and 16.5 mm over the 10-to-50 mm $Z_o$ range.

The Multimode SLIC-50 Transducer

Fig. 3 shows the geometrical arrangement and the diverging L- and S-beams of the multimode SLIC-50 transducer. The SLIC-50 was especially designed to yield two well separated and nearly equal strong signals (pulse 1 from the $Z_1$ location and pulse 2 from the $Z_2$ location) from an underclad fatigue crack. An additional crack-confirmation-and-sizing advantage of the SLIC-50 over the SLIC-40 is that the former transducer produces a pair of pulses (doublet) separated by a screen distance $\sigma$ that is practically independent of transducer position X (hence, "satellite pulse").

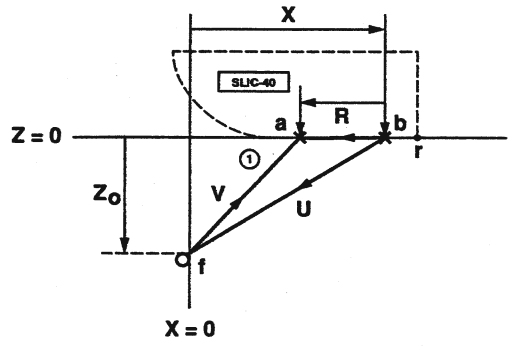


r: reference point for X measurements
b: exit point of probe B
f: sound reflecting point
X: lateral separation of points b and f (transducer position relative to point reflector)
U: sound path between points b and f
$Z_o$: Z location of point reflector
a: effective entry point of probe A (depends on $Z_o$)
R: lateral separation of points a and b (also sound path for time-reference pulse)
V: sound path between points a and f

Fig. 2. The three rays (U, V, and R) involved in the production of a strong L-wave signal (pulse 1) as a result of the interaction of the SLIC-40 with a side-drilled hole parallel to the Y-axis.

The primary function of this transducer is crack sizing. Fig. 3(a) actually shows the SLIC-50 in its traditional crack-sizing position $X_2$ [see also the right part of Fig. 3(b)] where the amplitude $A_2$ of the crack-depth-information-carrying signal (pulse 2) is maximum. Note that the satellite pulse is now the result of an L- to S-wave mode conversion at the lower crack extremity.

Fig. 4 shows the three sound paths (rays bf, fa, and ba) postulated for the stronger of the two interactions of the SLIC-50 with a side-drilled hole. The arrival time of the reference pulse traveling from point b to point a is given by Eq. (1). The variation of the flight time of the S-wave reflected by the hole (pulse 2) relative to the arrival time of the reference pulse with transducer position is calculated from

$$T_2\ (X;\ Z_o) = (U - R)/c + W/v \text{ in } \mu s \tag{4}$$

where

$$U\ (X;\ Z_o) = (Z_o^2 + X^2)^{1/2} \tag{4a}$$

and

$$W\ (X;\ Z_o) = \left[ Z_o^2 + (X - R)^2 \right]^{1/2}. \tag{4b}$$

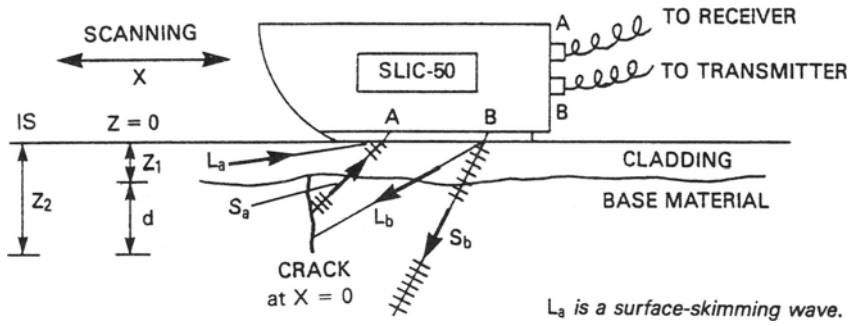


(a) Transmitted ($L_b$, $S_b$) and received ($L_a$, $S_a$) beams.

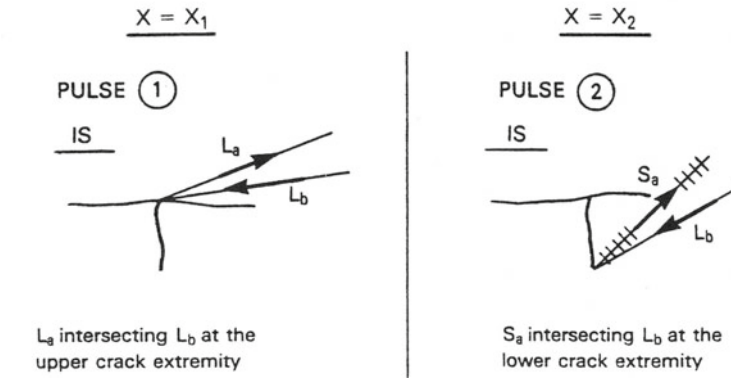


(b) Two pulses returned by an underclad crack.

Fig. 3. Interaction of the transmitted 60-degree longitudinal wave ($L_b$) of the SLIC-50 with an underclad crack resulting in four edge-diffracted pulses (one L-wave and one S-wave from each crack extremity). These pulses are labeled 1L or 1, 1S, 2L, and 2S or 2. The production of pulse 2L is the least efficient (diverging L-beams).

Here, v is the S-wave velocity. For the SLIC-50 used, the variation of the position of pulse 2 against the 50-mm wide instrument screen with transducer position X for a given reflector location $Z_o$ is predicted by

$$P_2 (X;Z_o) = 0.264 (U - R) + 0.488W \text{ in mm} \quad (5)$$

where R is taken to be 19 mm irrespective of $Z_o$.

The ray analytical model postulated for the weaker of the two interactions of the SLIC-50 with a side-drilled hole is similar to that shown in Fig. 2, since mode conversion is not involved in the production of pulse 1 by either the SLIC-50 or the SLIC-40. The variation of the flight time of pulse 1 relative to the arrival time of the reference pulse with transducer position is given by Eq. (2). For the SLIC-50 used in the experiments, the variation of the position of pulse 1 against the 50-mm wide instrument screen with transducer scanning for a given point reflector is predicted by

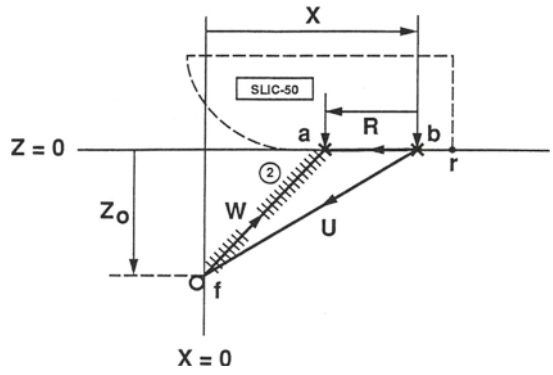


r: reference point for X measurements
b: exit point of probe B
f: sound reflecting point
X: lateral separation of points b and f (transducer position) relative to point reflector)
U: sound path between points b and f
$Z_o$: Z location of point reflector
a : effective entry point of probe A (depends on $Z_o$)
R : lateral separation of points a and b (also sound path for time-reference pulse)
W: sound path between points a and f

Fig. 4. The three rays (U, W, and R) involved in the production of a strong S-wave signal (pulse 2) as a result of the interaction of the SLIC-50 with a side-drilled hole parallel to the Y-axis.

$$P_1 (X;Z_o) = 0.264 (U + V - R) \text{ in mm} \quad (6)$$

where R is allowed to vary between 18 and 19 mm over the 10-to-50 mm $Z_o$ range.

The Multibeam SLIC-30 Transducer

This transducer was especially designed to detect and fully characterize buried ($Z_1$ > 30 mm) fatigue cracks in hard-to-inspect components. Fig. 1 (drawn for the SLIC-40) also serves to illustrate the interaction of the transmitted 50-degree longitudinal wave ($L_b$) of the SLIC-30 with a buried crack resulting in four edge-diffracted pulses (one L-wave and one S-wave from each crack extremity). These pulses are labeled 1L or 1, 1S, 2L or 2, and 2S. The S-wave pulses are generally not observed.

For the SLIC-30 used, the variation of the position of pulse 1 against the 50-mm wide instrument screen during transducer scanning for a known point reflector is predicted by

$$P_1 (X;Z_o) = 0.394 (U + V - R) \text{ in mm} \quad (7)$$

where R is allowed to vary between 16 and 18 mm over the 10-to-60 mm $Z_o$ range.

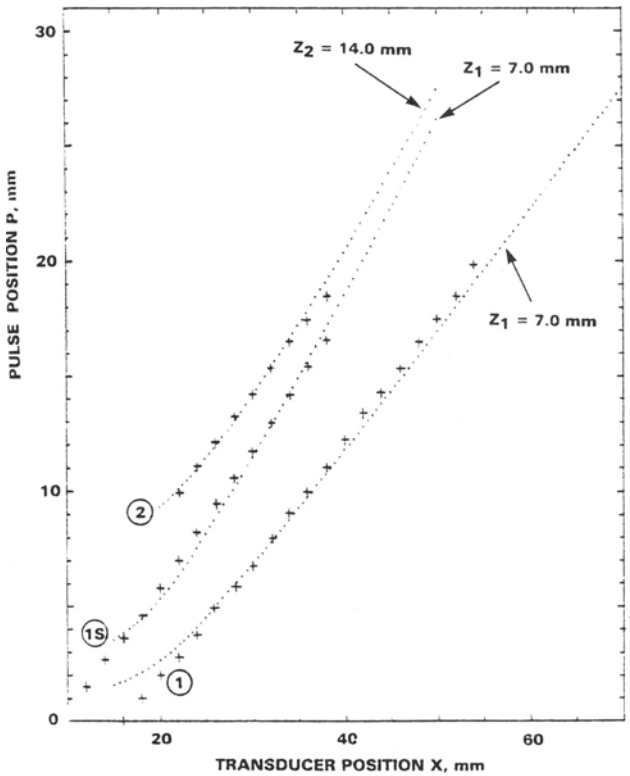


Fig. 5. The best fits of the computed SLIC-50 pulse vs. transducer position (PX) plots (•••) to the data (+++) obtained for a nominally 7-mm deep underclad fatigue crack ($Z_1$ = 7 mm, and $Z_2$ = 14 mm).

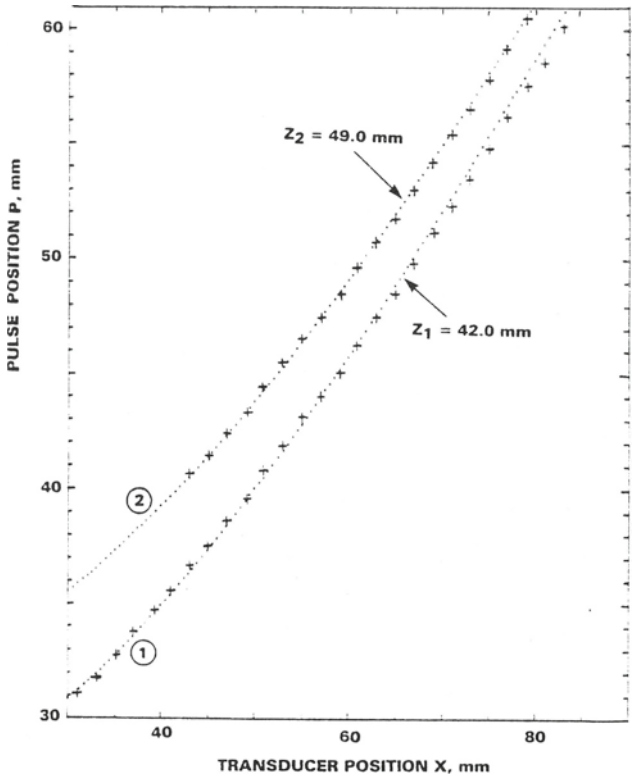


Fig. 6. The best fits of the computed SLIC-30 pulse vs. transducer position (PX) plots (•••) to the data (+++) obtained for a nominally 7-mm deep buried fatigue crack ($Z_1$ = 43 mm, and $Z_2$ = 50 mm).

## CRACK SIZING THROUGH INVERSE RAY TRACING

The SLIC-40/50/30 pulse position $P_i$ vs. transducer position X formulas [Eqs. (3), (5), (6), and (7)] were validated under blind test conditions by predicting with acceptable inaccuracy (±1 mm) the depth of fourteen fatigue cracks. Each crack was measured with each of the SLIC transducers from both the near (cladded surface) and the far (uncladded surface) sides to estimate its through-wall location ($Z_1$) and dimension ($d = Z_2 - Z_1$). The $Z_1$ and $Z_2$ extremity-location values for one of the nominally 7-mm deep cracks in a 57-mm thick cladded specimen were estimated by graphically fitting the measured $P_i(X)$ lines to a family of computed $P_i(X; Z_1 \text{ or } Z_2)$ lines as shown in Figs. 5 and 6. The intended $Z_1$ and $Z_2$ values for this crack were 7 and 14 mm respectively when the crack was viewed from the near side and 43 and 50 mm when it was viewed from the far side. The best fits between the computed and measured PX lines were obtained by the $Z_1$ and $Z_2$ values listed in Table 1 against their intended values.

Table 1

COMPARISON BETWEEN THE ESTIMATED AND (INTENDED) EXTREMITY LOCATIONS AND DEPTHS FOR A NOMINALLY 7-MM DEEP FATIGUE CRACK IN A CLADDED TEST SPECIMEN

| Transducer Configuration | SIDE OF EXAMINATION: Near | | | Far | | |
|---|---|---|---|---|---|---|
| | $Z_1$ (7mm) | $Z_2$ (14mm) | d (7mm) | $Z_1$ (43mm) | $Z_2$ (50mm) | d (7mm) |
| SLIC-40 | 8 | 15 | 7 | 42 | 49 | 7 |
| SLIC-50[a] | 7, 7 | 14 | 7 | 41 | 47 | 6 |
| SLIC-30[b] | 8 | 15 | 7 | 42 | 49 | 7 |

[a]See Fig. 5
[b]See Fig. 6

## REFERENCES


1. G. J. Gruber, D. R. Hamlin, H. L. Grothues, and J. L. Jackson, NDT International, 19, 155 (1986).
2. G. J. Gruber and J. A. G. Temple, in Proceedings of 4th European Conference on Nondestructive Testing, September 13-17, 1987, London, England.